Astronomy & Astrophysics manuscript no. aanda
January 15, 2022
©ESO 2022

arXiv:2004.03175v1 [astro-ph.GA] 7 Apr 2020

Letter to the Editor

Discovery of a Thirty-Degree Long Ultraviolet Arc in Ursa Major

A. Bracco[*1,2], R. A. Benjamin[3], M.I.R. Alves[4], A. Lehmann[2], F. Boulanger[2], L. Montier[5], D. Mittelman[6], D. di Cicco[6], and S. Walker[6]

[1] Rudjer Bošković Institute, Bijenička cesta 54, 10000 Zagreb, Croatia
e-mail: *abracco@irb.hr
[2] Laboratoire de Physique de l'Ecole Normale Supérieure, ENS, Université PSL, CNRS, Sorbonne Université, Université de Paris, Paris, France
[3] University of Wisconsin-Whitewater, Department of Physics, 800 West Main St, Whitewater, WI, 53190, USA
[4] Radboud University, Department of Astrophysics/IMAPP, P.O. Box 9010, 6500 GL Nijmegen, The Netherlands
[5] IRAP, Université de Toulouse, CNRS, CNES, UPS, Toulouse, France
[6] MDW Sky Survey, New Mexico Skies Observatory, Mayhill, NM 88339, USA

Received: March 17, 2020; Accepted: April 3, 2020

ABSTRACT

Our view of the interstellar medium of the Milky Way and the universe beyond is affected by the structure of the local environment in the Solar neighborhood. Here, we present the discovery of a thirty-degree long arc of ultraviolet emission with a thickness of only a few arcminutes: the Ursa Major Arc. It consists of several arclets seen in the near- and far-ultraviolet bands of the GALEX satellite. A two-degree section of the arc was first detected in the Hα optical spectral line in 1997; additional sections were seen in the optical by the team of amateur astronomers included in this work. This direction of the sky is known for very low hydrogen column density and dust extinction; many deep fields for extra-galactic and cosmological investigations lie in this direction. Diffuse ultraviolet and optical interstellar emission are often attributed to scattering of light by interstellar dust. The lack of correlation between the Ursa Major Arc and thermal dust emission observed with the *Planck* satellite, however, suggests that other emission mechanisms must be at play. We discuss the origin of the Ursa Major Arc as the result of an interstellar shock in the Solar neighborhood.

Key words. Diffuse Ultraviolet emission, Interstellar Medium, Radiative Shocks, Supernova Remnants, Galactic foregrounds

1. Introduction

New observations of the diffuse interstellar medium (ISM) in 21-cm emission, dust emission and polarization, and low radio frequency polarized emission, have awakened new interest in linear structures in the ISM that may affect our view of the Solar neighborhood (Clark et al. 2015; Jelić et al. 2015; Planck Collaboration Int. XXXII 2016). The study of the structure of the local and diffuse ISM is important as it provides a foreground that must be accounted for in studying our Milky Way and the universe beyond.

In 2001 P. McCullough & R.A. Benjamin presented the discovery of an unusually straight and narrow ionized 2°.5-long filament detected in Hα (656 nm, hereafter the MB filament) — with a surface brightness of ∼0.5 R — in the direction of Ursa Major (McCullough & Benjamin 2001, hereafter MB01), whose origin is yet to be established. They considered four options for the origin of this structure: (1) a low-density jet, (2) an unusually straight nebular filament, (3) shock ionization by a compact source, e.g. a neutron star, and (4) a trail of ionized gas left by a low-luminosity ionizing source. Although they favored the final "Fossil Stromgren Trail" (FST) option, no plausible ionizing source was ever identified.

In this letter we present the outstanding discovery of a longer portion of the MB filament seen both in the ultraviolet and in Hα extending over thirty degrees on the sky. We discuss its origin in terms of interstellar shocks in the ISM.

2. Description of the Ursa Major (UMa) Arc

We investigated the MB filament in several wavebands using the Aladin sky-viewer (Boch & Fernique 2014) and discovered that the MB filament is also visible both in the Far Ultraviolet (FUV; 130-180 nm) and in the Near Ultraviolet (NUV; 170-280 nm) bands of the Galaxy Evolution Explorer (GALEX) All-Sky Imaging Survey (AIS) (Bianchi 2009). The Ultraviolet imaging, which covers a much wider area of the sky than the original Hα observations, demonstrates that the MB filament is a piece of a much larger arc-like structure. A GALEX FUV image displaying a large fraction of the Ursa Major Arc (UMa Arc) is shown in Fig. 1 along with zoom-in views of selected sections in Hα and the GALEX NUV band. The structure consists of several piecewise-continuous arclets, occasionally multiple. Most of the arclets we found lie along a curved path from Galactic coordinates (l, b) = (115°.4, 30°.7) to (147°.7, 43°.5).

If the structure were due to a linear trail, the option favored by MB01, it would project onto a great circle on the sky. We found that no single great circle can fit the arc we observed. In addition, a search of GALEX images of nearby white dwarfs and hot subdwarfs with parallaxes and proper motions measured by the Gaia satellite (Geier et al. 2019) shows no structures in the FUV similar to the original MB filament. For these two reasons, the FST hypothesis appears to be ruled out.

We have found instead that most of the arclets lie along one-sixth (1 radian) of a circle centered on (l, b) = (107°.7, 60°.0) with angular radius Θ_R = 29°.28 ± 0°.23, labeled as Feature

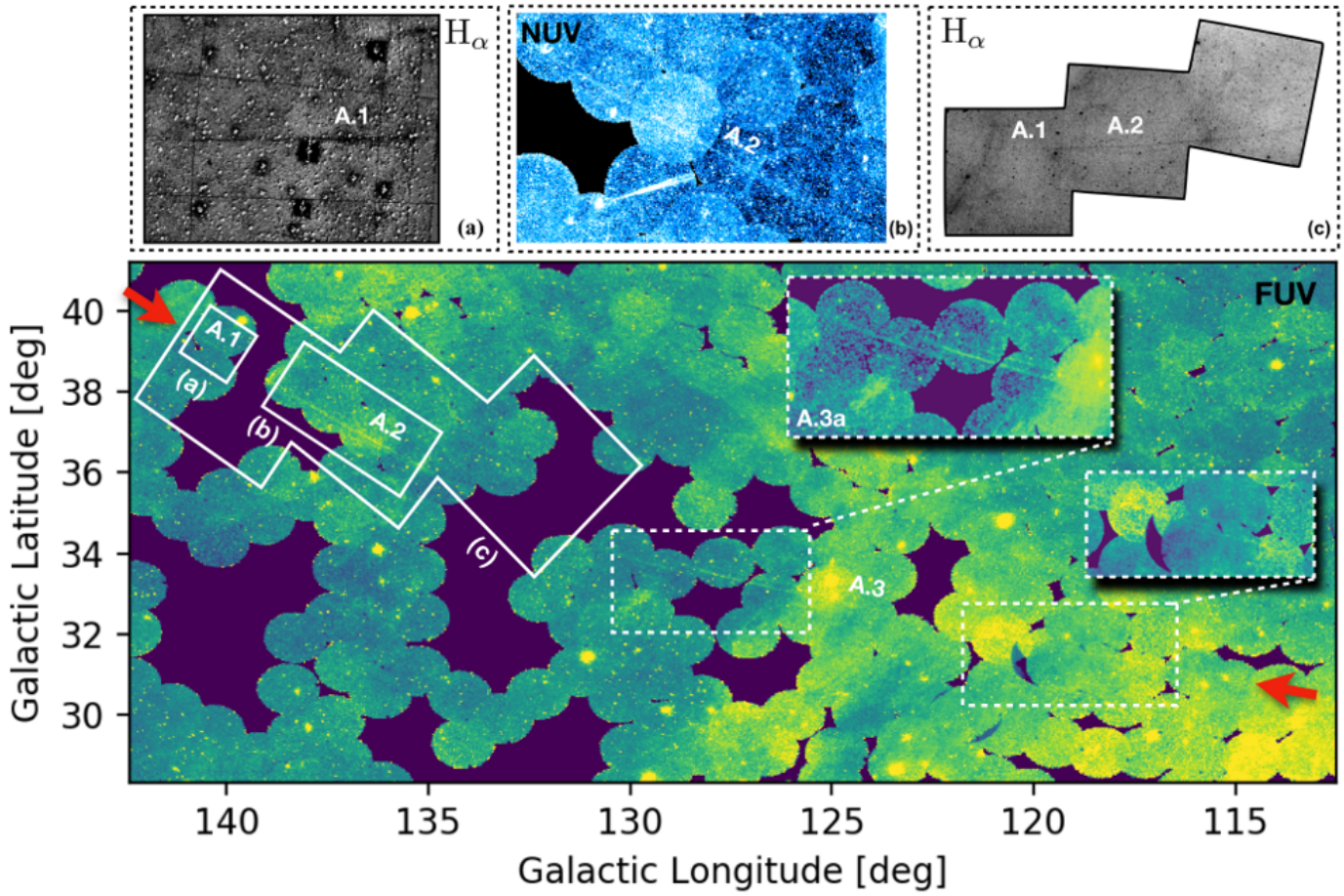


Fig. 1. *The Ursa Major (UMa) Arc, Feature A (between the red arrows), in a mosaicked image of GALEX FUV data taken in 2005. Each (circular) pointing has a diameter of* 1°.27. *Inset (a) shows the original 1997 detection of the Hα filament published by McCullough & Benjamin (2001); inset (b) shows part of the arc in GALEX NUV data; inset (c) shows a section of the arc that was observed in Hα as part of the MDW Hydrogen-Alpha Sky Survey in 2016 (Mittelman et al. 2019). The bright NUV feature below A.2 is an artifact in the GALEX data. Intensity scaling in all diagrams is arbitrary. In general, brighter colours correspond to more intense regions in the FUV and NUV maps, while darker colours correspond to more intense Hα. We label the three sections of this feature as A.1, A.2, and A.3 interrupted by gaps in the GALEX coverage. The two additional insets in the FUV maps along A.3 have an adapted color scale to optimize the visualization of the arcs.*

A in Fig. 1. If one three-degree long arclet, centered at (l, b) = (131°,+33°.7) (the lowest arclet in A.3a in Fig. 1), is not considered, the standard deviation drops to σ_Θ = 0°.18 or 0.6% of the angular radius. The individual arclets are even thinner, ranging from 0.3 to a few arcminutes. An extrapolation of this arc — the UMa Circle — encircles a total area of 2681 square degrees (0.25π steradians), 6.5% of the total sky and 27% of the sky above Galactic latitude b = 32°. The angular size of this full region is comparable to the largest angular size radio-continuum loops discovered in the 1960s (Quigley & Haslam 1965). What distinguishes the UMa Arc compared to these other structures is (1) the thickness-to-radius ratio, (2) the nearly perfect circular fit over thirty degrees of arc, and (3) the high Galactic latitude of the center.

Figure 2 shows the positions of the arclets and the UMa Circle on a stereographic projection, overlaid on the total gas column density derived from *Planck* observations of thermal dust emission (Planck 2013 results. XI. 2014). A visual search of the GALEX mosaics identified three additional high-latitude arclets: two (Feature B.1 and B.2, centered at (l, b) = (79°,+52°)) lie interior to the UMa circle; only one (Feature C, centered at (l, b) = (185°,+53°)) lies outside this region (see also Fig. C.1). Also overlaid in Fig. 2 are the locations of several previously claimed loops, shells, and arcs based on radio continuum observations (Radio Loop III) (Quigley & Haslam 1965), studies of dust emission (North Celestial Loop/GS135+29+4) (Meyerdierks et al. 1991), and 21-cm observations (Intermediate Velocity Arch/GS155+38-58 (Kuntz & Danly 1996) plus additional Heiles shells (Heiles 1984)). None of these shells — which are far less well delineated than the UMa Arc — are clearly aligned with the arc we observe. We also investigated the Effelsberg-Bonn HI Survey (EBHIS) (Winkel et al. 2016) and found no evidence for a 21-cm counterpart to the Hα, or ultraviolet, emission. For visualization purposes we also present the UMa Arc and Circle in Fig. C.2.

The region within the UMa Circle is well known for having the lowest column densities of neutral hydrogen in the sky, including the "Lockman Hole" (Lockman et al. 1986), which lies 5°.4 interior to the arc. This low column density region is part of a vertically extended, tilted low-density cavity identified as the "Local Chimney" (Welsh et al. 1999). The low column density and the large angular size of the UMa Circle also make it a potentially important foreground for extra-galactic and cosmological studies, requiring a thorough characterization of the interstellar emission interior and exterior to the arc.

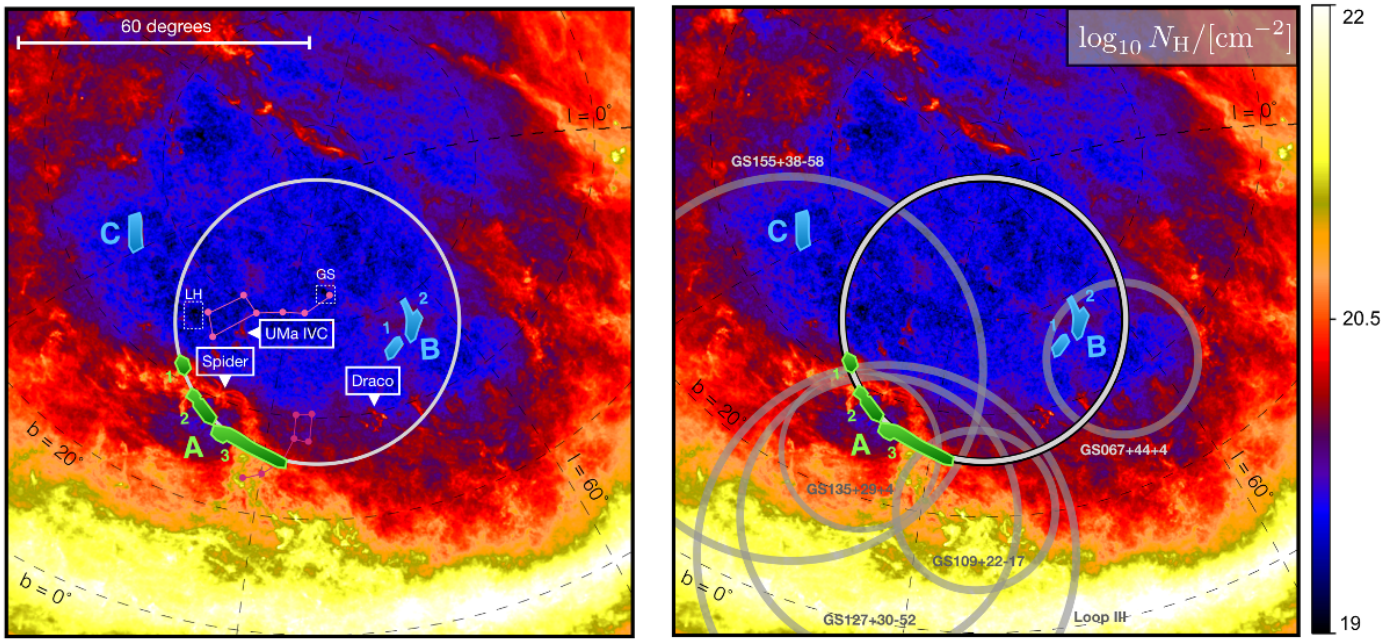


Fig. 2. *Stereographic projection of the total gas column density, $N_{\rm H}$, derived from Planck observations of dust thermal emission (color scale). The locations of Feature A, which defines the UMa Arc, and Features B and C are marked. The UMa Circle is shown in light gray. The left panel gives the positions of the UMa IVC, Draco, and Spider clouds, along with the Ursa Major and Minor constellations (in pink). Two of the lowest column-density windows in the Galaxy (Lockman hole (LH) and Groth strip (GS)) are shown. The right panel indicates the positions of known arches and loops, in dark gray. The transition between blue and red on the false-colour intensity scale corresponds to $N_{\rm H} = 10^{20}$ cm^{-2}.*

Locating the UMa Arc along the line of sight is not trivial given the data in hand. The large angular size suggests its proximity. The presence of three well-known interstellar clouds that lie — in projection — within the UMa Circle may be also indicative: the UMa molecular intermediate-velocity cloud (IVC), the Spider cloud, and the Draco molecular IVC, with distances of 356±20 pc, 369±22 pc, and 481±50 pc, respectively (Zucker et al. 2019). If the Draco cloud were physically inside the UMa Arc, it would imply that the center of this structure is more than 350 pc above the Galactic midplane with a radius larger than 200 pc. Given all these caveats and the large angular size of the structure, the UMa Arc cannot be further than a few hundred pc from the Sun.

3. The ultraviolet emission of the UMa Arc

In the following, we examine the source of the UV emission from the UMa Arc. Analyses of high latitude diffuse ultraviolet emission using both FIMS/SPEAR (on the STSAT-1 korean satellite) and GALEX have shown that FUV emission is generally highly correlated with 100 μm dust emission — due to dust scattering — and somewhat correlated with Hα intensity (Seon et al. 2011). Figure 3 shows the same section of Feature A in FUV (top panel) and in dust optical depth (bottom panel) as traced by the *Planck* observations at 850 μm. While areas of enhanced dust emission, S.1 and S.2, in the *Planck* image are associated with an increase in FUV brightness, presumably due to dust scattering, the UMa Arc features, A.1 and A.2, are clearly not associated with dust emission. This is also confirmed by the average FUV/NUV ratio that we computed along the A.2 portion of the Arc. As detailed in Appendix A, we measured the ratio using perpendicular profiles to the FUV and NUV filaments in the GALEX maps and averaging them along their full length. We found a ratio of 0.31 ± 0.05, which is significantly smaller than the values expected for dust scattering, mostly larger than unity (Murthy et al. 2010).

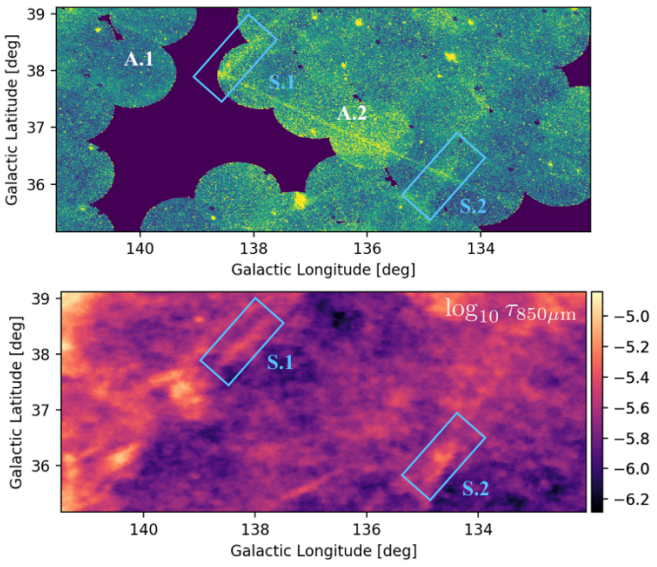


Fig. 3. *Comparison between the GALEX FUV data (top panel) and the dust optical depth ($\tau_{850\mu m}$, bottom panel), derived from the dust thermal emission measured by Planck at 850 μm. Regions S.1 and S.2 are identified in both FUV and dust emission, whereas features A.1 and A.2 are only seen in FUV emission.*

If not associated with dust scattering, other sources of diffuse FUV emission must be considered including the two-photon continuum emission from hydrogen, ion-atomic emission lines, e.g., C IV λ 154.8/155.1 nm, He II λ 164.0 nm, and O III] λ 166.2 nm, and fluorescent molecular hydrogen emission lines.

4. Is the UMa Arc a shock front?

Ion lines are proxies of hot gas (with temperatures > 10^4 K) likely produced in the cooling zone of interstellar shocks with velocities larger than 50 km/s (Nishikida et al. 2006). Recombination of the post-shock gas would produce as well two-photon emission contributing to the UV continuum. Radiative shocks are expected to be a key source of dissipation of kinetic energy driven by supernova blast waves in the ISM, making supernova remnants (SNRs) the most favorable scenario for the formation of structures such as the UMa Arc.

To test this idea we inspected GALEX FUV images of four large angular-diameter ($\Theta_R > 10°$) old SNRs: the Monogem Ring (Plucinsky et al. 1996), Antlia SNR (McCullough et al. 2002), G70.0-21.5 (Fesen et al. 2015) and G353-34 (Testori et al. 2008). The first two objects have been the targets of low angular resolution FUV spectroscopy with FIMS/SPEAR (Shinn et al. 2007). All four objects show networks of thin FUV filaments reminiscent of the UMa Arc, but over a smaller solid angle of the sky; two of these, Antlia SNR and G070.0-21.5, have also been shown to have similar Hα filaments. In Fig. C.3 we show the case of G070.0-21.5 in Hα, FUV, and dust emission.

The geometry of the arclets, the emission in the GALEX NUV and FUV channels, and the concomitant Hα are all consistent with the hypothesis that the UMa Arc is a shock, or pressure front, created by an explosion, yet unknown, towards $(l, b) = (107°.7, 60°.0)$. The thinness and multiplicity of the structures could be produced by the edge-on projection of corrugated sheets in the front and post-shock recombination zones, similar to what is seen in the Cygnus Loop SNR (Hummer & Storey 1987; Raymond et al. 1988). If this hypothesis was true then the UMa Arc could be associated to a corrugated edge on sheet of the Loop III SNR (see Fig. 2).

With the caveat that the radius of curvature of an individual arc is not always the same as the radius of curvature of the full remnant, we can compare the UMa Arc to expectations of a simple model of blast wave evolution for a SNR (Draine 2011). Under the assumption that the UMa Arc is a section of a front centered on a point $d_{100} = d/(100\text{pc})$ from the Sun and using a standard explosion energy of $E_{SN} = 10^{51}$ ergs, the remnant will still be in the adiabatic phase — with shock speed greater than 190 km/s — if the ambient density is $n_{H,0} < (0.17\text{cm}^{-3}) d_{100}^{-2.38}$. Alternately, for an assumed ambient density of $n_{H,0} = 1$ cm^{-3}, the remnant would have transitioned to a pressure-modified momentum-conserving snowplow[1] phase with an age of $t_{snow} = (0.7\,\text{Myr}) d_{100}^{3.5}$ and a front speed that is approaching the random ISM velocity.

Assuming that the ambient density was sufficiently high to trace a radiative front, we computed a series of shock models from publicly available libraries (Sutherland & Dopita 2017) with shock velocities between 50 km/s and 400 km/s, pre-shock interstellar magnetic-field strengths between 1 μG and 10 μG, and mean diffuse gas density in the pre-shock medium of 0.1 cm^{-3}. These models allow us to predict the level of emission — both lines and continuum — within the GALEX bandpasses at the shock front that we can compare to the observed FUV/NUV ratio.

As shown in the top row of Fig. 4, we identified two possible domains that reproduce the observations delimited by the 1-σ contour of the measured FUV/NUV ratio. Shocks at intermediate velocities (between 50 km/s and 100 km/s) and at high velocity (> 300 km/s) are both consistent with the measured value of 0.31 ± 0.05. These two regimes, however, show opposite line-to-continuum ratios, that is, only at intermediate velocities (<100 km/s) the two-photon continuum emission dominates over the ion-line contribution. The level of two-photon emission predicted by these models is also consistent with the analytical derivation of the FUV/NUV count ratio of 0.37 that can be found in Appendix B. This intermediate velocity range is favored as well by the predicted Hα surface brightness (see the top-right panel in Fig. 4) that compares well with the value of 0.5 R measured in 1997 (McCullough & Benjamin 2001). Nonetheless, notice that our models do not take into account limb-brightening projection factors that alter the estimate of the Hα surface brightness (Hummer & Storey 1987). Additional constraints are therefore needed and may come from future spectral observations of ion lines (i.e. O III], SII, and NII) toward the UMa Arc, which, as predicted by our models and presented in the bottom row of Fig. 4, will reveal opposite line ratios relative to Hα in the two velocity regimes.

[1] In this phase the energy radiated behind the shock front is comparable to the initial energy of the explosion.

5. Conclusions

In this letter we reported the stunning discovery of the UMa Arc, or one of the largest and diffuse structures of the Northern sky, yet unknown until now. We discussed the possibility that the UMa Arc is the relic of a radiative shock in the neighborhood of the Sun (< few hundred pc). Future work will be crucial to better constrain the physical parameters of the UMa Arc, as well as its distance, both for understanding our local astrophysical environment and for properly describing the structure of the Galactic ISM as a foreground for extra-galactic and cosmological studies. It will be necessary to (1) measure the Hα radial velocity along the length of the Arc, (2) to constrain the proper motion of the MB filament since the original 1997 observations, and (3) search for associated interstellar absorption lines to bracket the distance to the structure. Finally, future observational data, including optical/UV emission line spectra to obtain shock parameters, will put additional constraints on the presumed front.

Acknowledgements. We thank the anonymous referee for her/his comments. We would like to acknowledge Peter McCullough as the original discoverer of the MB filament which led to this work nearly twenty years later. We also thank the organizers of the 2018 program Milky-Way-Gaia of the PSI2 project funded by the IDEX Paris-Saclay, ANR-11-IDEX-0003-02, where this work started. We thank David Schiminovich for advice on calculating GALEX count-rates and John Raymond and Jon Slavin for useful discussions about GALEX data and supernova remnants. We would also like to acknowledge the hard work and untimely passing of David Mittelman in 2017, who strongly contributed to the realization of the MDW survey. We thank as well Bruce Draine and Peter G. Martin for comments to the manuscript. A.B. acknowledges the support of the Agence Nationale de la Recherche (project BxB: ANR-17-CE31-0022) and funding from the European Union's Horizon 2020 research and innovation program under the Marie Skłodowska-Curie Grant agreement No. 843008. A.B. thanks as well the game of *la marelle* https://www.youtube.com/watch?v=8c4tsQvRNWY to help breaking his quarantine walls. M.I.R.A acknowledges funding from Radboud University (Excellence Fellowship); R.A.B. acknowledges the support of NASA grant NNX17AJ27G. This research has made use of "Aladin sky atlas" developed at CDS, Strasbourg Observatory, France.

References

Bianchi, L. 2009, Astronomy and Astrophysics Supplement, 320, 11
Boch, T. & Fernique, P. 2014, in Astronomical Society of the Pacific Conference Series, Vol. 485, Astronomical Data Analysis Software and Systems XXIII, ed. N. Manset & P. Forshay, 277
Clark, S. E., Hill, J. C., Peek, J. E. G., Putman, M. E., & Babler, B. L. 2015, Physical Review Letters, 115, 241302
Draine, B. T. 2011, Physics of the Interstellar and Intergalactic Medium

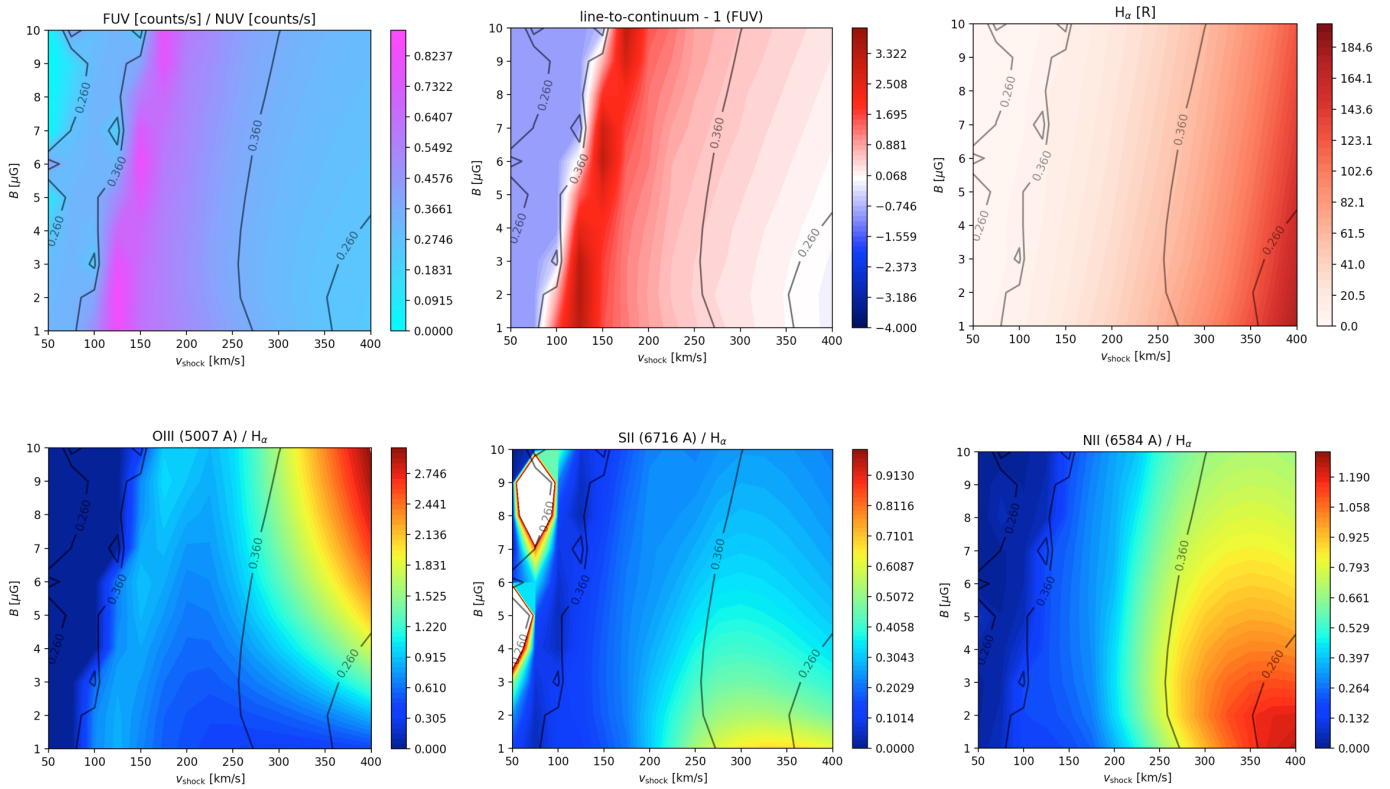


Fig. 4. *Grid of models of radiative shocks from Sutherland & Dopita (2017) with varying magnetic-field strengths and shock velocities in a diffuse medium with pre-shocked density of* 0.1 cm^{-3}. *Top row: FUV/NUV ratio from the models (left), line/continuum ratio in the GALEX FUV bandpass (center, similar behaviours are found in the NUV case), Hα emission (right). The line to continuum ratio is centered around 0 so that blue (red) colours correspond to larger (smaller) continuum emission compared to line emission. Bottom row: ion line to Hα ratios for OIII (left), SII (center), and NII (right). In all six panels the black contours represent the 1-σ level of the observed FUV/NUV of* 0.31 ± 0.05.

Fesen, R. A., Neustadt, J. M. M., Black, C. S., & Koeppel, A. H. D. 2015, Astrophysical Journal, 812, 37
Geier, S., Raddi, R., Gentile Fusillo, N. P., & Marsh, T. R. 2019, Astronomy and Astrophysics, 621, A38
Hamden, E. T., Schiminovich, D., & Seibert, M. 2013, Astrophysical Journal, 779, 180
Heiles, C. 1984, Astrophysical Journal, 55, 585
Hummer, D. G. & Storey, P. J. 1987, Monthly Notices of the Royal Astronomical Society, 224, 801
Jelić, V., de Bruyn, A. G., Pandey, V. N., et al. 2015, Astronomy and Astrophysics, 583, A137
Kuntz, K. D. & Danly, L. 1996, Astrophysical Journal, 457, 703
Lockman, F. J., Jahoda, K., & McCammon, D. 1986, Astrophysical Journal, 302, 432
McCullough, P. R. & Benjamin, R. A. 2001, Astronomical Journal, 122, 1500
McCullough, P. R., Fields, B. D., & Pavlidou, V. 2002, Astrophysical Journall, 576, L41
Mellinger, A. 2009, PASP, 121, 1180
Meyerdierks, H., Heithausen, A., & Reif, K. 1991, Astronomy and Astrophysics, 245, 247
Mittelman, D., di Ciccio, D., & Walker, S. 2019
Murthy, J., Henry, R. C., & Sujatha, N. V. 2010, Astrophysical Journal, 724, 1389
Nishikida, K., Edelstein, J., Korpela, E. J., et al. 2006, ApJ, 644, L171
Nussbaumer, H. & Schmutz, W. 1984, Astronomy and Astrophysics, 138, 495
Planck 2013 results. XI. 2014, Astronomy and Astrophysics, 571, A11
Planck Collaboration Int. XXXII. 2016, A&A, 586, A135
Plucinsky, P. P., Snowden, S. L., Aschenbach, B., et al. 1996, Astrophysical Journal, 463, 224
Quigley, M. J. S. & Haslam, C. G. T. 1965, Nature, 208, 741
Raymond, J. C., Hester, J. J., Cox, D., et al. 1988, Astrophysical Journal, 324, 869
Seon, K.-I., Witt, A., Kim, I.-J., et al. 2011, Astrophysical Journal, 743, 188
Shinn, J.-H., Min, K. W., Sankrit, R., et al. 2007, Astrophysical Journal, 670, 1132
Spitzer, Lyman, J. & Greenstein, J. L. 1951, Astrophysical Journal, 114, 407
Sutherland, R. S. & Dopita, M. A. 2017, ApJS, 229, 34
Testori, J. C., Reich, P., & Reich, W. 2008, Astronomy and Astrophysics, 484, 733
Welsh, B. Y., Sfeir, D. M., Sirk, M. M., & Lallement, R. 1999, Astronomy and Astrophysics, 352, 308
Winkel, B., Kerp, J., Flöer, L., et al. 2016, Astronomy and Astrophysics, 585, A41
Zucker, C., Speagle, J. S., Schlafly, E. F., et al. 2019, ApJ, 879, 125

Appendix A: Measuring the FUV/NUV ratio from the GALEX data

We computed the ratio between the FUV and NUV bands for the straightest/longest portion of the UMa Arc (A.2 in Fig. 1) using the mosaics of the GALEX All-Sky Survey that were delivered by the GALEX team to the Mikulski Archive for Space Telescopes (MAST) and can be found at https://archive.stsci.edu/prepds/gcat/gcat_dataproducts.html with further documentation at http://www.galex.caltech.edu/wiki/GCAT_Manual.

In order to account for visible offset variations among the different tessellations of the mosaic (see Fig. 1), we computed the FUV/NUV ratio by correlating average UV fluxes perpendicular to the main crest of A.2 (see Fig. A.1), labeled < FUV > and < NUV >, respectively. With the caveat that offsets were uniform within each tessellation, any miscalibration among the mosaics would be captured by the intercept of the linear fit between < NUV > and < FUV >, while the slope would correspond to the actual ratio between the two frequency bands.

In the right panel of Fig. A.1 we show the linear fit and the corresponding slope of 0.31 ± 0.05 obtained for the pixels that correspond to the position of A.2 (orange data points). As shown by the green profile in the left panel of the same figure, the linear fit allows us to strikingly reproduce the observed < FUV > profile from the observed < NUV >.

Appendix B: Theoretical estimate of the two-photon emission

Below we calculate the expected GALEX countrate for two-photon emission, which is expected to produce a fixed ratio of FUV to NUV emission (Spitzer & Greenstein 1951). For two-photon emission, the Case B emissivity per unit frequency (ergs s^{-1} cm^{-2} sr^{-1} Hz^{-1}) is given by (Draine 2011)

$$j_\nu^B(2s \rightarrow 1s) = j_\nu^{2s,B} = \frac{1}{4\pi} n_e n_p \alpha_{eff}^{(2s)B}(T) \left[h\nu P_\nu^{2s}\right], \quad \text{(B.1)}$$

where n_e, n_p are the electron and proton densities, $\alpha_{eff}^{(2s)B}(T)$ is the total recombination to the hydrogen $2s$ level, where we use the data for Case B recombination (Hummer & Storey 1987), and $[h\nu P_\nu^{2s}]$ is the energy emitted per frequency interval for the two-phton continuum. The recombination rate to the $2s$ level is one-third of the total recombination rate, where we use a fit to the temperature dependence (Draine 2011): $\alpha_{eff}^{(2s)B}(T) = (1/3)(2.59\times 10^{-13}$ cm^3 s^{-1}) $f^{2s}(T)$ where $f^{2s}(T) = T^{-0.833-0.035\ln T_4}$ and $T_4 = T/10^4$ K. We use an analytical fit to the spectral shape of the two photon continuum (Nussbaumer & Schmutz 1984): $\left[h\nu P_\nu^{2s}\right] = hyA(y)/A_{2s\rightarrow 1s}$, where $y = (\nu/\nu_{Ly\,\alpha})$ is the frequency scaled by the Lyman α frequency, $A_{2s\rightarrow 1s} = 8.2249$ s^{-1} is the Einstein A value for the two-photon decay, and

$$A(y) = C\left[y(1-y)(1-(4y(1-y))^\gamma + \alpha(y(1-y))^\beta(4y(1-y))^\gamma)\right], \quad \text{(B.2)}$$

with $C = 202.0$ s^{-1}, $\alpha = 0.88$, $\beta = 1.53$, and $\gamma = 0.8$. It is also convenient to define the unitless function $B(y) = A(y)/202.0$ s^{-1}.

Taken together, for a constant density path length, L, with an emission measure of $EM = n_e n_p L$, the two-photon continuum intensity per frequency interval, $I_\nu^{2s,B} = \int j_\nu^{2s,B} ds$ is

$$I_\nu^{2s,B}(y,T,EM) = (3.45\times 10^{-21} \text{ ergs s}^{-1}\text{ cm}^{-2}\text{ sr}^{-1}\text{ Hz}^{-1})\times \times f^{2s}(T) y B(y) \left[\frac{EM}{\text{cm}^{-6}\text{ pc}}\right] \quad \text{(B.3)}$$

Similarly, the Case B recombination Hα intensity can be written as

$$I^{H\alpha,B}(T,EM) = (8.71\times 10^{-8} \text{ ergs s}^{-1}\text{ cm}^{-2}\text{ sr}^{-1})\, f^{H\alpha}(T) \left[\frac{EM}{\text{cm}^{-6}\text{ pc}}\right], \quad \text{(B.4)}$$

where $f^{H\alpha}(T) = T_4^{-0.942-0.031\ln T_4}$. Expessed in Rayleighs (R), the Hα intensity is $I^{H\alpha,B}(T,EM) = (0.36\ R) f^{H\alpha}(T)$ [EM/cm^{-6} pc]. For $T = 8000$ K, this yields the oft-used conversion that $1R$ corresponds to $EM = 2.25$ cm^{-6} pc.

In wavelength units, $\lambda_{\text{Å}} = \lambda/(1\text{Å})$, where $y = 1215/\lambda_{\text{Å}}$, the two-photon continuum intensity is given by

$$I_\lambda^{2s,B}(y,T,EM) = (1.04\times 10^{-2} \text{ ergs s}^{-1}\text{ cm}^{-2}\text{ sr}^{-1}\text{ Å}^{-1})\times \times f^{2s}(T) y B(y) \lambda_{\text{Å}}^{-2} \left[\frac{EM}{\text{cm}^{-6}\text{ pc}}\right]. \quad \text{(B.5)}$$

To calculate the bandpass weighted continuum intensities, $I_{band} = \int T_{band}(\lambda) I_\lambda^{2s,B} d\lambda \;/\; \int T_{band}(\lambda) d\lambda$ we use the intensity formula above together with the effective area curves, $T_{band}(\lambda)$, from http://www.galex.caltech.edu/researcher/effective_area/. For an emission measure of $EM = 1$ cm^{-6} pc at $T = 8000$ K, this yields $I_{band} = 3.6$ and 1.4×10^{-10} ergs s^{-1} cm^{-2} Å^{-1} sr^{-1} for the FUV and NUV channels, respectively. Using the standard GALEX conversion (Hamden et al. 2013) from energy units (ergs s^{-1} cm^{-2} Å^{-1}) to countrate (counts s^{-1}), and assuming a pixel size of $(12.88)^2$ arcsec^2 yields a predicted GALEX countrate of $C_{band} = (0.98$ and 2.61×10^{-3} counts s^{-1} pixel^{-1}) [EM/cm^{-6} pc] for the FUV and NUV channels, resulting in a predicted FUV/NUV count ratio for two-photon continuum emission of 0.37.

Appendix C: Supporting figures

In this appendix we show a series of figures to support the main body of the paper.

Figure C.1 shows Features B and C introduced in Sect. 2.

In Fig. C.2, for visualization purposes, we show a large-scale stereographic projection of the UMa Arc and Circle (in red) on top of the Mellinger full-sky map (Mellinger 2009). The loops and shells already presented in Fig. 2 are shown in light blue.

For comparison with the UMa Arc, Fig. C.3 presents the SNR G070.0-21.5 introduced in Sect. 4. It shows the SNR in Hα from the MDW survey, in FUV from GALEX, and in dust optical depth from *Planck*. As for the UMa Arc, an intertwined network of filaments can be seen in Hα and FUV without any counterpart in dust emission. This supports the interpretation of the ultraviolet emission from the UMa Arc as the product of a process different than dust scattering in the diffuse ISM.

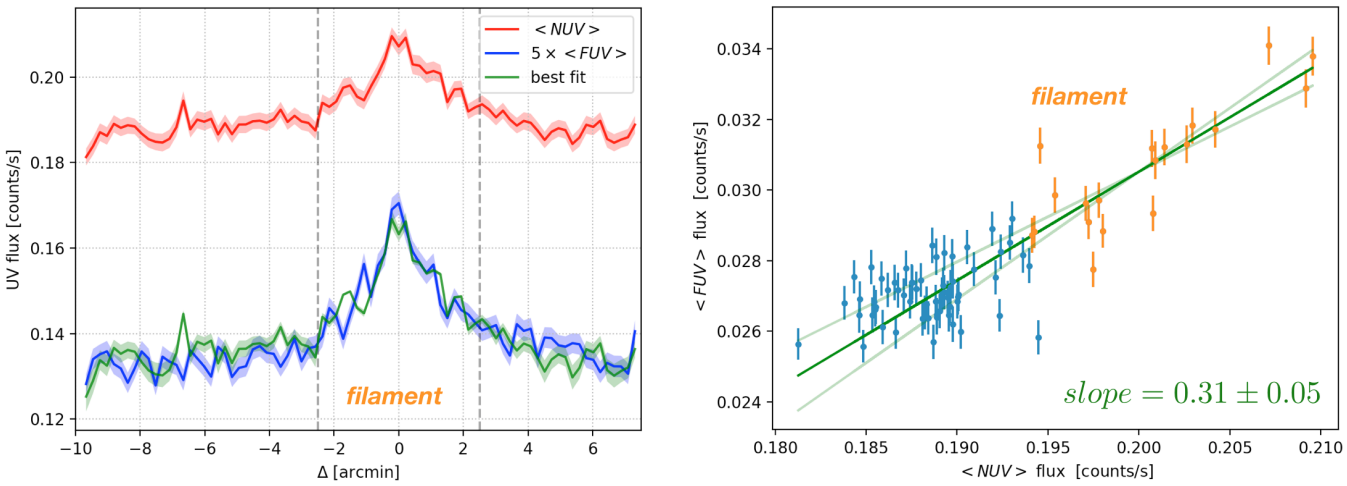


Fig. A.1. *Left panel: FUV (blue) and NUV (red) intensities, averaged over the whole length of A.2 (see Fig. 3), versus position across the width in arcmin. We show the average profiles, labeled < FUV > and < NUV >, and their corresponding errors. < FUV > is scaled up for visualization purposes, as well as the best-fit profile shown in green (see main text and right panel). Two vertical dashed lines delimit the borders of the A.2 filament merging with the local background/foreground UV emission. Right Panel: scatter plot and linear correlation between < FUV > and < NUV >. The linear fit was computed only considering the data points (see orange circles) within the vertical dashed lines in the left panel. The intensity profile obtained scaling the < NUV > with the best-fit parameters of the linear fit is shown in green on the left.*

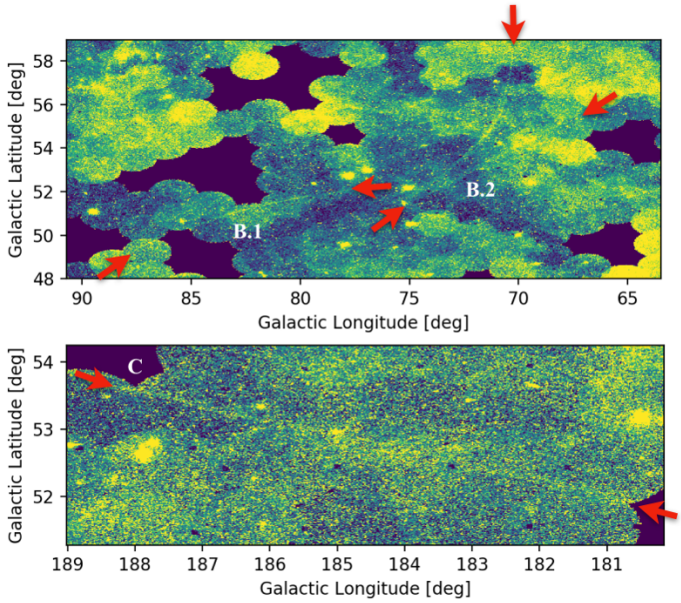


Fig. C.1. *Features B (top) and C (bottom) in a mosaicked image of GALEX FUV data.*

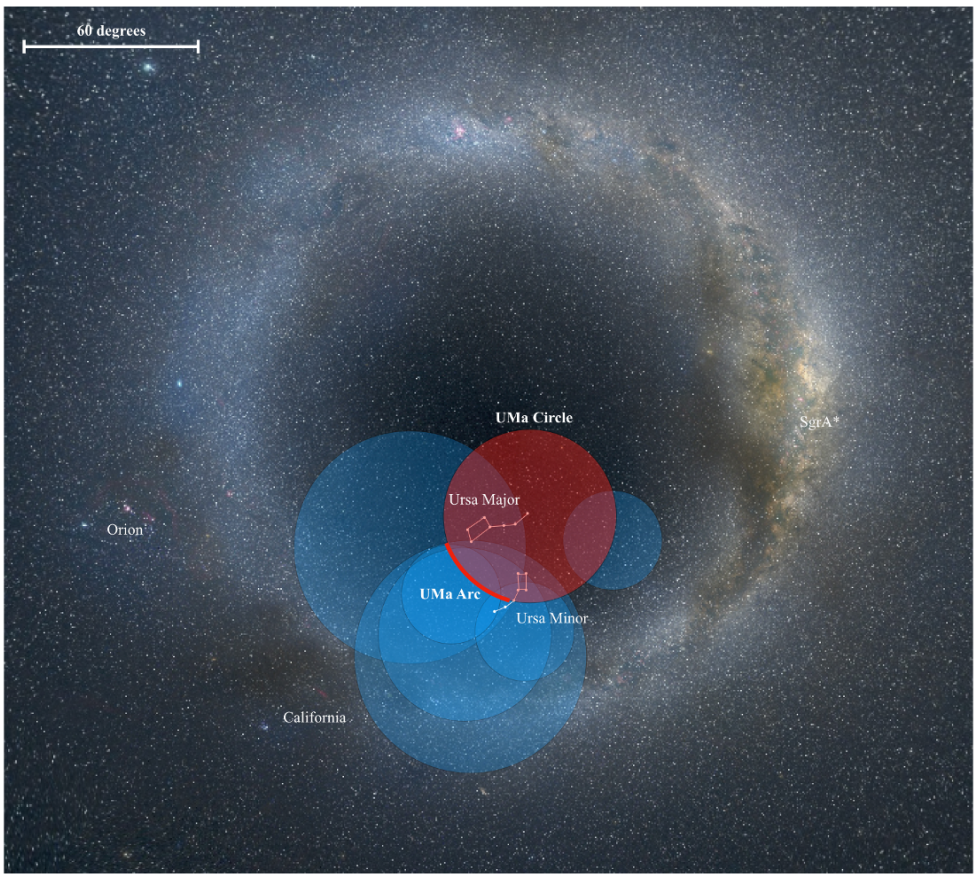


Fig. C.2. *Large-scale stereographic overview of the UMa Arc and Circle (red) on top of the Mellinger full-sky map. We also show as reference the positions of the loops and shells presented in Fig. 2 in light blue as well as some known constellations and the Galactic center (SgrA*).*

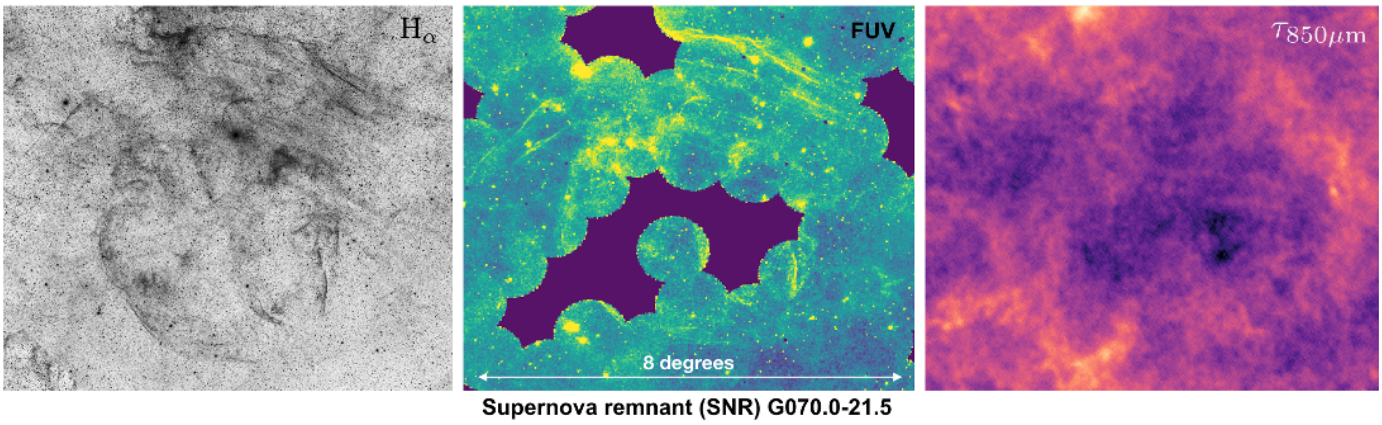


Fig. C.3. *SNR G070.0-21.5 (see Sect. 4) in Hα from the MDW survey (left), in FUV from GALEX (centre), and in dust optical depth from Planck (right).*